UNIVERSITY OF
BATH

University of Bath

Investigation of Mechanical Loss and Heat Transfer in an Axial-Flux PM Machine

Rafal Wrobel[1], Gyula Vainel[2) 4)], Colin Copeland[3], Tomasz Duda[3], Dave Staton[4] and Phil Mellor[1]

[1] Department of Electrical & Electronic Engineering
University of Bristol
Bristol, UK
r.wrobel@bristol.ac.uk

[2] ThyssenKrupp Presta Hungary Ltd.
Budapest, Hungary
gyula.vainel@thyssenkrupp.com

[3] Department of Mechanical Engineering
University of Bath
Bath, UK
c.d.copeland@bath.ac.uk

[4] Motor Design Ltd.
Ellesmere, UK
dave.staton@motor-desig.com

Abstract— **This paper investigates components of the mechanical loss together with heat transfer effects in an axial-flux PM motor. The mechanical loss components generated within electrical machines are well known, however, their prediction or derivation has not been widely reported in the literature. These, together with the electromagnetic loss sources and heat transfer effects are crucial and must be accounted for when considering high-power density, high-speed and/or compact machine design.**

This research is focused on separating the mechanical loss components to gain a more in depth understanding of the effects and their importance. Both experimental and theoretical techniques have been employed in the analysis. In particular, hardware tests with dummy rotors have been performed to measure the bearing and windage/drag loss components. These have been supplemented with CFD analysis to theoretically evaluate the aerodynamic effects occurring within the mechanical air-gap accounting for loss and heat transfer.

Further to these, a 3D lumped parameter thermal model of the axial-flux PM demonstrator has been developed to validate predictions of the mechanical loss components and heat transfer mechanisms. The theoretical findings show good agreement with experimental data. Moreover, the research outcomes suggest that the mechanical and aerodynamic effects require careful consideration when a less conventional machine design is considered.

I. INTRODUCTION

There are a number of works investigating various aspects of the axial-flux PM machines including the electromagnetic and/or thermal phenomena [1]–[10]. The thermal and parasitic loss effects are receiving increased attention due to the drive towards high-power dense, compact and efficient machine designs for automotive and aerospace applications. In addition there has been an upsurge of interest in axial-flux machines due to their potential for greater torque density and more compact construction as compared with their radial-flux counterparts. However, thermal analysis of the axial-flux machines is less developed and understood than that of the radial-flux machine topologies [6]-[11].

The general laws governing thermal phenomena within electrical machines provide an initial estimation of the machine's thermal behaviour. However, as developments in materials and manufacturing techniques allow less conventional machine constructions to be considered feasible, more comprehensive and detailed analysis of prototype machines becomes essential. This results from the design, manufacture and assembly nuances that are difficult to account for without experimentally derived data.

The mechanical loss components associated with the aerodynamic effects have not been widely investigated in the literature in the context of machine design methodology. These machine design aspects are difficult to analyse in a timely and generic manner. The existing research is limited to selected aspects of these effects, which are usually considered at the later stages of the design process if found to be significant. The majority of work in the field is devoted to more demanding machine designs with forced air- or liquid-cooling of the rotor or rotor/stator assembly [6]-[10], [19]-[24]. The importance of understanding the rotor windage/drag and heat transfer mechanisms has been acknowledged and investigated for various machine designs [6]-[10], [19]-[29]. Further to this, the rotor/stator air-gap convective heat transfers phenomena regarding the axial-flux machine topology have been researched in detail, providing valuable insight into the heat transfer correlations [6]-[9], [11].

The bearing loss has had some attention in the context of testing techniques and related life span prediction [13]-[17]. All the existing methods of predicting the bearing loss are based on empirical formulae and do not account for the specifics of the applications they were used in [13]-[17]. The bearing loss and rotor aerodynamic effects become increasingly important when considering compact high-performance machine designs.

This paper focuses on the mechanical loss components together with rotor heat transfer effects occurring in an axial-flux PM machine demonstrator. This main research theme is supplemented with selected aspects of the thermal analysis

and testing methodology used in development of the prototype machine. The experimentation involves thermal tests and loss measurements whereas the theoretical investigation makes use of computational fluid dynamics (CFD) and lumped-parameter thermal equivalent circuit techniques. The lumped-parameter method employed here utilises a cuboidal element approach accounting for three-dimensional (3D) heat transfer, material thermal anisotropy and internal heat generation [12]. Both thermal analysis techniques have been employed here to investigate the thermal behaviour of the prototype motor. Further to this, CFD has been used to evaluate the aerodynamic (windage/drag) loss component. The presented research outcomes confirm the importance of the mechanical and aerodynamic effects when considering compact machine design. In particular, careful consideration must be taken when designing the mechanical bearing arrangement. Moreover, an appropriate aerodynamic rotor design might allow for improved air-gap heat transfer and consequently allow a higher power output capability for the motor.

II. MOTOR DEMONSTRATOR

The research has been focused on a single-sided axial-flux brushless PM motor. The stator core is manufactured using a soft magnetic composite (SMC) with 12 slots ($q = 12$) and double layer concentrated winding, whereas the rotor assembly includes 10 PM poles ($p = 10$). The PM poles are segmented and surface mounted on the rotor back iron disc. The rotor is fully enclosed within the motor casing. The stator core together with the winding is encapsulated using high thermal conductivity resin (≈ 1W/m·K) providing good conductive heat transfer into the motor casing. Figs. 1 and 2 illustrate the outline of the motor topology together with a photograph of the prototype. Table I presents basic motor data.
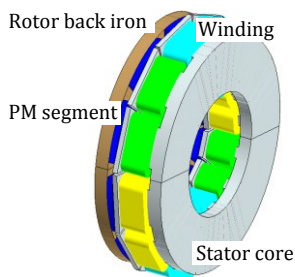

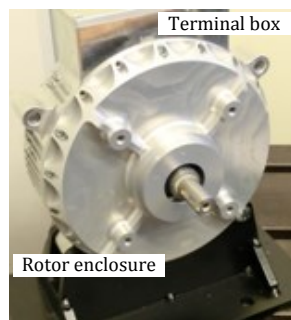Fig. 1. Outline of the PM axial-flux motor topology

Fig. 2. Prototype motor

Table I. Basic Motor Data

Peak power	14.9kW
Peak torque	70.0Nm
Peak speed	6000rpm
Peak efficiency	> 90.0%
DC link voltage	72.0V
Dimensions	$\varnothing$237.0mm × 130.0mm

The machine is intended to operate with natural air-cooling. Such a motor construction imposes some challenges regarding heat transfer within the rotor-enclosure. In particular, heat extraction from the rotor assembly is limited due to low air flow/air movement. Furthermore, the mechanical arrangement of the bearings is integrated within the stator assembly which allows for a compact machine design and cost/time effective manufacture/assembly, but results in an elevated operating temperature of the bearings and potential difficulties with setting and maintaining an appropriate bearing preload. These effects are discussed later in the paper.

III. MECHANICAL LOSS COMPONENTS

In general, the mechanical power loss generated in electrical machines has two components: bearing loss and aerodynamic loss. The loss components are attributed to contact friction effects in the bearing assembly and to the machine's rotating/moving parts interacting with the surrounding fluid/air respectively.

A. Bearing Power Loss

There are a wide variety of bearing types which rely upon the rolling action of balls or rollers. In general, a bearing provides a low friction constrained motion from one body relative to another. A typical bearing construction includes five components: inner and other rings with raceways, rolling elements, cage and seal [13], [14]. The rolling elements are contained between the inner and outer rings providing a connection between the rings with a minimum contact surface area. A cage is used to ensure a uniform distribution of the rolling elements and to prevent their mutual contact. The raceways store a lubricant and prevent axial motion of the elements. A seal is commonly used to contain the lubricant and protect the raceways from contamination.

The bearing loss has two basic loss components attributed to rolling friction and sliding friction. These are caused by various phenomena occurring within the bearing assembly during its operation and include: elastic hysteresis in rolling, sliding due to deformation of contacting elements and/or bearing geometry, spinning of rolling elements, gyroscopic pivotal motion of the rolling elements, sliding between the cage and rolling elements and between the cage and bearing rings, viscous friction due to lubricant motion and seal friction [14]. These fundamental effects are well known, however due to their complexity they are difficult to quantify. A majority of these phenomena vary during the life span of the bearing, which is caused by the bearing operating conditions/environment, bearing preload, long term bearing wear effects and maintenance schedule among others. Existing theoretical techniques of predicting bearing loss are based on empirical formulae with several non-deterministic input parameters [14]. Therefore, an experimental approach accounting for the statistical scatter of measured data derived under nominal operating conditions seems the most appropriate here. However, such a method is time and

resource intensive and in the case of electrical machines the bearings must be tested in situ within the machine in order to account for the specific mechanical and preload arrangement of the bearings including any magnetic forces.

B. Windage/Drag Power Loss

The aerodynamic power loss component is frequently referred to as windage loss. In general, this loss component is generated by friction resulting from relative fluid/air movement in reference to the machine's rotating parts, e.g. rotor structure, air-gap, end-windings cooling cavity and internal and external fanassemblies among others. This aerodynamic interaction originates from three fundamental effects that contribute to the overall windage power loss: skin friction, pressure drag and induced drags [30]. However, these effects are difficult to predict individually in a generic and computationally effective manner. The existing analytical approximations applicable to the design of electrical machines are based on accumulated experience and/or empirically adjusted formulae [24]. These techniques are limited to specific machine topologies and operating conditions. A more generic approach makes use of CFD modelling techniques [6]-[9], [21].

Understanding and accurately predicting this power loss component is particularly important in high-speed and forced air cooled machine designs [6]-[9], [21]. Windage power loss is less significant in more conventional machine designs, however, the thermal aspects of such machine designs are strongly dependent on the aerodynamic effects and resulting heat transfer mechanisms within the motor's air-gap and end-winding cavity [6]-[9], [21]-[24]. There are various correlations available allowing for these heat transfer effects to be accounted for in the design process. However, the existing correlation techniques require some degree of calibration using experimental data and are limited to a particular class of machine topology and construction. An approach utilising a CFD modelling technique is more generic, but requires a degree of calibration to ensure accuracy and consistency.

IV. EXPERIMENTAL SETUP

To assess the mechanical loss together with the aerodynamic and heat transfer effects two dummy rotors have been manufactured, see Fig. 3. The dummy rotor with surface protrusions is representative of the surface mounted PM rotor assembly used in the prototype, whereas the second dummy rotor with a flat, even surface is representative of analytical and experimental studies reported in the literature. Both dummy rotors have been manufactured using non-magnetic and non-electrically conductive material (Tufnol). The machine assembly has been fully instrumented with a number of type-K thermocouples including the inner and outer surfaces of the rotor- enclosure. The test regime includes rotational tests with dummy rotors at open-circuit to derive the mechanical loss (bearing and windage/drag loss) and with DC winding excitation to provide insight into the heat transfer within the motor air-gap.
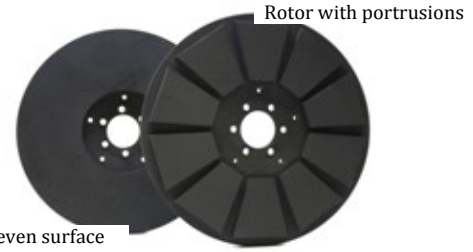

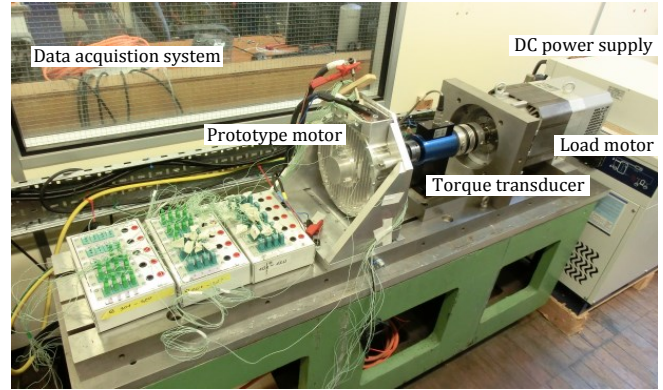Fig. 3. Dummy rotor assemblies

Fig. 4. Experimental setup

Tests with the rotor assembly removed from the motor body have been performed to assess the bearing loss only. It is important to note the tests with dummy rotors do not account for any electromagnetic interaction between the stator and rotor assemblies occurring during motor operation. It is expected that in some cases this interaction might lead to further bearing loss due to mechanical load variation. However, this effect is difficult to quantify in a simple manner utilising the existing hardware and is not considered here.

The experimental setup used in the analysis includes the motor under test, torque transducer and load machine working here as a prime mover, see Fig. 4.
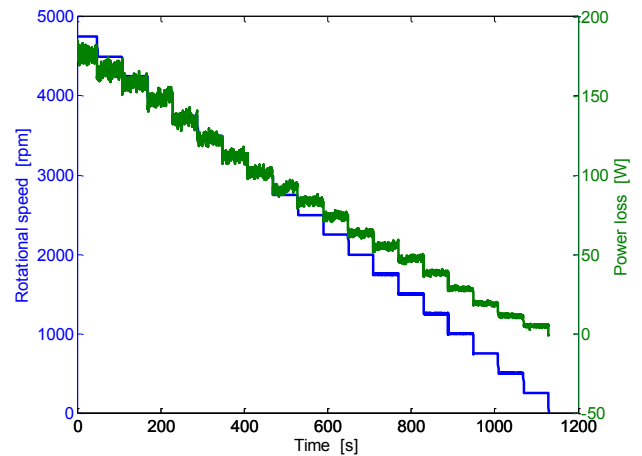

Fig. 5. An example of measured mechanical data loss set

All the components have been mounted on a custom-built precision finished test bed with locating and aligning features. These are particularly important to avoid erroneous torque readings due to torque offset and provide repeatable measuring conditions when performing several tests with various motor/rotor assemblies. A single data capture for a particular motor/rotor assembly includes instantaneous torque, rotational speed, mechanical power, temperatures and DC winding power loss where appropriate. These are recorded for the rotational speed increments for both clockwise (CW) and counter clockwise (CCW) rotational direction to compensate for potential torque offset/torque measurement error. Moreover, a data set for consecutive rotational speeds is collected over a fixed time interval and used to average the mechanical loss measurements. Fig. 5 presents an example of mechanical loss data set from tests on the hardware motor.

I. MATHEMATRICAL MODELS

A. Computational Fluid Dynamics (CFD)

A three-dimensional (3D) CFD has been employed to evaluate some of the effects discussed earlier. In particular, the aerodynamic loss and heat transfer effects are investigated here. A reduced model approach has been used, where the fluid space enclosed by the rotor, stator and rotor-enclosure is modelled. In addition, due to periodic symmetry, only one tenth of the rotor/rotor-enclosure is represented within the 3D CFD model. Fig. 6 shows the full model domain divided with rotational periodicity as well as the surface mesh of the rotor and shaft. The fluid domain mesh has been created with ANSYS ICEM CFD 14.0 using a fully hexahedral mesh consisting of 1,027,000 cells. Owing to the different turbulent regimes that are expected to exist throughout the speed range, two different turbulence models have been tested, namely, K-epsilon and shear stress transport (SST). At low rotational speeds, purely laminar models were also created. The non-dimensional first node distance from the wall, namely the y^+ value, was set to or below unity.
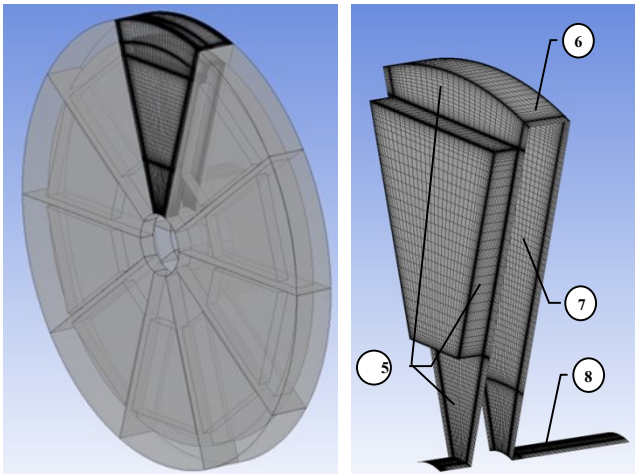

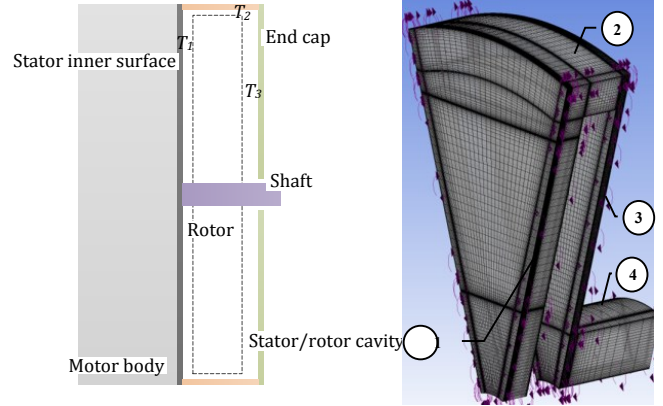Fig. 6. 3D CFD model representation of the rotor/rotor-enclosure

Fig. 7. Cross-section of the motor demonstrator showing the temperature measurements and the corresponding 3D CFD model representation

The boundary conditions were informed by thermocouple temperature measurements made using the experimental setup presented in Fig. 4. Fig. 7 shows the general measurement locations and the corresponding boundary conditions applied to the fluid domain.

Note that since this is a fully enclosed fluid domain, no inlet or exit boundary conditions were needed. However, the fluid domain was initialized to standard atmospheric conditions before converging to the final steady-state solution. The stator temperature boundary condition (position 1) was assumed to be a linear radial temperature distribution between two sets of thermocouple measurements located on the stator surface near the end-cap (maximum radius) and hub (minimum radius). For the other inner casing surfaces (position 2 and 3 in Fig. 7) a constant average temperature was deemed sufficient. The remaining boundary surfaces were prescribed an adiabatic boundary condition. The model movement was set up with no-slip boundary conditions applied to all surfaces, with the rotor surfaces rotating to match the experimental results.

Note that although most runs where able to reach the convergence criterion of RMS residuals $\leq 10^{-5}$, this target was difficult to reach under some conditions, as will be outlined in the results section.

B. Lumped Parmeters Thermal Model

A 3D lumped parameter thermal model of the motor demonstrator has been constructed using the cuboidal element approach [12] and implemented in PORTUNUS [34]. Such a model definition allows for the 3D heat transfer, material thermal anisotropy and internal heat generation to be accounted for. The equivalent network has a multi-layer structure containing all the motor sub-regions/sub-assemblies. These include the winding, stator tooth/slot, stator back iron, rotor PM, rotor back iron, aluminium housing, shaft, bearing assembly and air-gap. Due its complexity and volume it is not possible to present the complete thermal network in a single schematic. Figs. 8 and 9 outlines the rotor and housing model representation only, as these are of particular interest in this analysis.
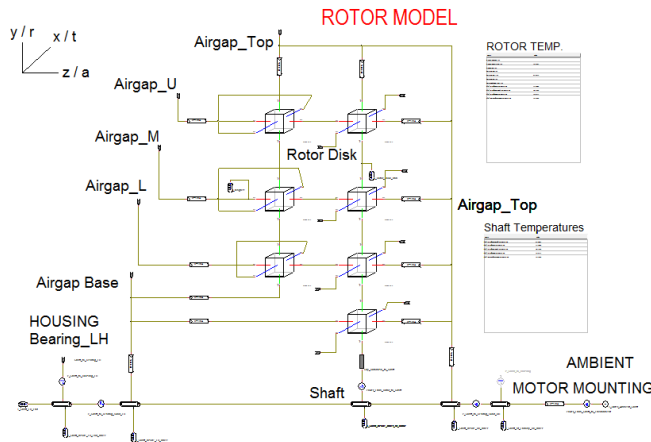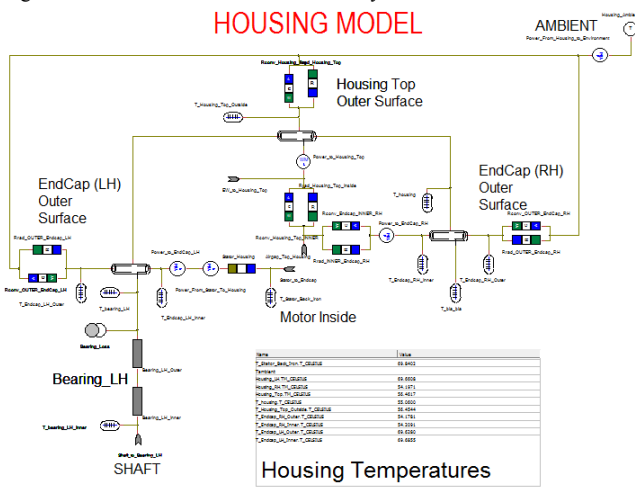
Fig. 8. Thermal model of the rotor assembly

Fig. 9. Thermal model of the housing assembly

Note that the model utilises the circumferential symmetry of the stator assembly, thus a single section of the motor containing a complete stator slot with winding has been analysed here. The rotor model representation shown in Fig. 8 is made up with several cuboidal elements [12] with 3D thermal heat paths accounting for the bearing assembly, air-gap, end-cap and surrounding ambient air. The model implementation accounts for the main heat transfer mechanisms occurring in the machine assembly, conduction, convection and radiation where appropriate.

Since the stator/winding assembly is encapsulated with high thermal conductivity resin, the conductive heat transfer from the stator/winding assembly into the motor aluminium casing is the major heat transfer mechanism here. However, as the rotor assembly is fully enclosed it is important to account for and understand the convective heat transfer phenomena within the rotor-enclosure. This is particularly important as the elevated rotor temperature has several implications regarding the machine's power output capabilities and reliability.

The model representation of the motor housing is shown in

Fig. 9 and accounts for the bearing assembly and related heat paths and the interfacing thermal resistances. The material thermal properties used in the analysis have been derived experimentally or obtained from manufactures data [12].

II. RESULTS AND DISCUSSION

A series of tests have been carried out to measure the mechanical loss. Fig. 10 presents the measured bearing loss at different temperatures versus rotational speed. The results suggest relatively high bearing loss when compared to the motor's power output capability. Moreover, these initial measurements indicate a degree of change in the bearing loss with temperature. However, more generic observations and statements regarding thermal dependence of the bearing loss is difficult to make based on this limited data. An experimental approach accounting for the statistical distribution of the data and a wider range of temperatures would be more appropriate, however, this might not be feasible if a standard evaluation procedure of a prototype machine is used, as is the case in this analysis.

In the experiment, the bearing assembly temperature was set by energising the stator wingding with DC excitation and adjusting it to achieve the required temperature. Here, two test points, 40^{0}C and 100^{0}C were analysed. The rotor assembly has been removed from the motor body prior to the tests. It is important to note that in the analysed motor demonstrator a set of two sealed ball bearings, deep grove radial and angular contact were used. In particular, the angular contact bearing was used to transfer the axial load resulting from interaction between stator and rotor assemblies.

Initial tests on the dummy rotor disc with smooth surfaces indicated no discernible increase in loss. Thus only results are presented for the dummy rotor with protrusions. Fig. 11 shows measured mechanical loss data from tests with this dummy rotor emulating the original rotor assembly.
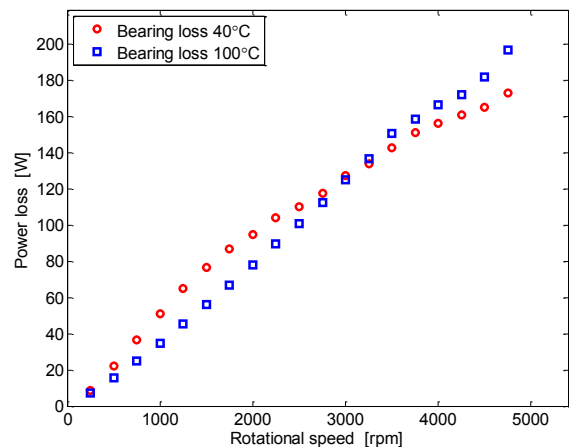

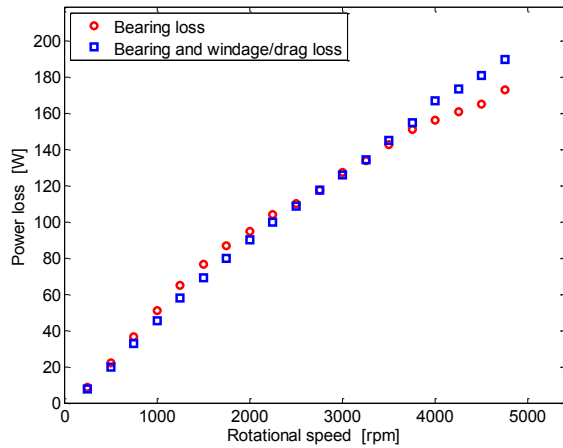Fig. 10. Measured bearing power loss versus rotational speed

Fig. 11. Measured mechanical power loss versus rotational speed

These results have been compared against the bearing loss data from previous tests. Both data sets correspond to the same bearing temperature, here 40^0C. When analysing the data, some increase in mechanical loss at higher speeds is evident. This may be attributed to the windage loss.

To have a more in-depth insight into the aerodynamic loss, a series of CFD analyses have been performed. In order to embark on a CFD study of a rotating fluid cavity, it is important to establish whether the fluid is laminar, turbulent, or a transitional phase between the two regimes. This is most often assessed using two non-dimensional parameters, the ratio of the stator-rotor gap and the tip radius ($G=g/R$) and the rotational Reynolds number ($Re_\theta = \omega R^2/\nu$), where ω is the angular velocity in rad/s and ν is the kinematic viscosity of ambient air. These calculations are provided in Table II. The authors that have studied transition in annular rotor stator cavities do not identify a clear transition from laminar to turbulent flows, in part due to the complexity of the instabilities that can develop. Four flow regimes have been proposed by Daily and Nece [32] where for G ≈ 0.012, a merged boundary layer transitions from laminar to turbulent $Re_\theta \approx 4.0\times10^4$. At G ≈ 0.025, the transition occurs at $Re_\theta \approx 1.0\times10^5$. Schouveiler et. al. [31] describes a more complex series of instabilities that can appear as low as $Re_\theta \approx 6.0\times10^4$ for G=0.02. However, Howey et. al. [8], [9] suggests a transition to turbulent flow for $Re_\theta \approx 3.0\times10^5$ for G ≈ 0.01.

Table II. Rotational Reynolds Number

G (g/R) – magnet/stator	0.0156	
G (g/R) – back side rotor/stator	0.0260	
RPM	Ang. velocity (rad/s)	Rotational Reynolds No. (Re_θ)
500	52.40	3.31×10^4
1500	157.10	9.92×10^4
2500	261.80	1.65×10^5
3500	366.50	2.31×10^5
4500	471.20	2.97×10^5

This highlights one of the most significant hindrances to attempting to model an axial flux machine in CFD. If the transition from laminar to turbulent for 0.015 < G < 0.025 could be in the range between $4.0\times10^4 < Re_\theta < 3.0\times10^5$, this covers most of the operating range in Table II. This can be very problematic since, as pointed in [33], the existing turbulent transition closure models can be unstable, and computationally expensive. The approach here will be to provide data for two different turbulence models (K-epsilon and SST) from 2000rpm - 4500rpm, and laminar solutions from 500rpm - 1500rpm. This assumes an abrupt laminar to turbulent transition at $Re_\theta \approx 1.0\times10^5$.

Fig. 12 provides the windage/drag power loss results from the CFD simulation as a function of rotational speed. As noted above, the data is populated by a laminar model from 500rpm-1500rpm and two turbulence models between 2000rpm-4500rpm. In addition, the K-epsilon turbulence model was tested below 2000rpm to understand the sensitivity of the prediction to the assumption of transition. When analysing results from the CFD analysis, similar trends of the windage/drag power loss have been observed
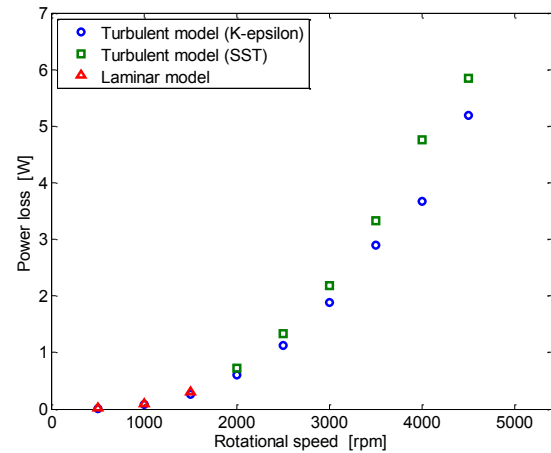

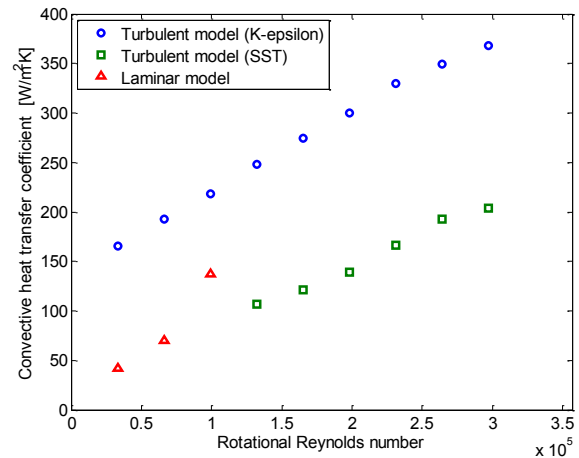Fig. 12. CFD prediction of windage/drag loss

Fig. 13. Convective heat transfer coefficient versus rotational Reynolds number
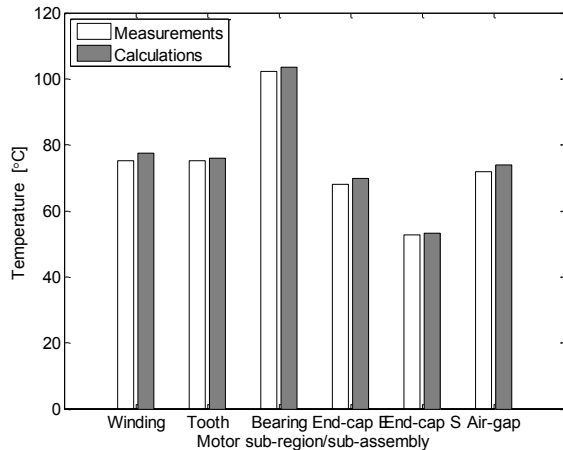
Fig. 14. Measured and calculated temperatures within selected motor sub-regions/sub-assemblies at $n = 4500$rpm $P_{electrical} = 88$W, $P_{mechanical} = 162$W

Fig. 15. Normalised winding temperature versus rotational speed for various bearing loss levels

for the adopted models. It has been shown that the windage/drag loss generated within the analysed motor assembly is relatively minor compared to the bearing loss thus confirming earlier results from tests on the motor demonstrator.

Fig. 13 shows the air-gap convective heat transfer coefficient predicted from the CFD model using the area averaged air gap temperature as the reference condition. This choice contrasts the widespread use of the ambient reference condition for forced or natural air convection cooling. Unlike the windage loss, the prediction of convection show significant discrepancy between the two turbulent models. In particular, the K-epsilon model suggests significantly higher convective heat transfer effects than the SST and laminar models. This reflects the importance in appropriately modelling the wall velocity gradient which determines the heat flux, and therefore the convective heat transfer coefficient. It also illustrates the importance of using caution in treating CFD simulations as a substitute for experimentally derived values. Considering the motor construction and the authors' previous experience, the results from the SST and laminar models seems more representative to phenomena occurring in the hardware demonstrator. This is also reflected by the experience expressed by other authors [8], [33].

The equivalent circuit thermal model of the machine demonstrator has been calibrated with data from tests outlined earlier. Fig. 14 presents an illustration of measured and calculated temperatures within the motor sub-regions/sub-assemblies for a single test point showing good correlation. Here, rotational speed is $n = 4500$rpm, electrical power loss within the motor winding $P_{electrical} = 88$W and mechanical power loss is $P_{mechanical} = 162$W.

In order to give some insight into the heat transfer phenomena within the motor air-gap/rotor-enclosure a sensitivity analysis has been carried out. Initially a low value of convective heat transfer representative of the locked/stationary rotor test has been used, 10W/m²K -
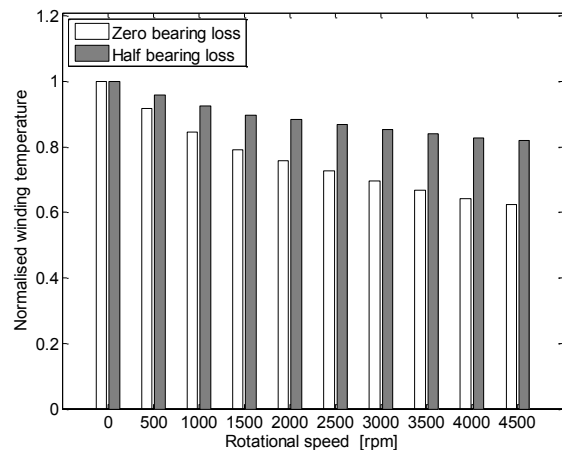
25W/m²K, and later a CFD predicted heat transfer coefficient has been introduced. To illustrate, an increase of the heat transfer coefficient to the maximal predicted value, 376W/m²K, only resulted in a 3% temperature drop for the winding. This confirms that the conductive heat transfer mechanism dominates in the stator assembly. In this analysis, the power loss generated in the rotor assembly for the complete motor is not accounted for. However, it is expected that this effect will have some impact on the overall heat transfer from and within the rotor-enclosure. These phenomena have not been investigated at this stage of the research.

To evaluate the severity and demonstrate the importance of the mechanical loss/bearing loss in the analysed motor prototype, a series of thermal analyses have been carried out for various bearing loss levels. Two case scenarios have been assumed here, zero bearing power loss and half of the original bearing loss. Predictions of the winding temperature from these analyses have been compared against the original data where the complete bearing loss is accounted for. Fig. 15 presents the normalised winding temperature indicating a significant reduction of the winding temperature at higher speed for both analysed case scenarios. This confirms importance of the mechanical/bearing loss components in design/analysis of the compact/high-performance electrical machines.

III. CONCLUSIONS

Mechanical power loss has a significant impact on a motor performance, yet very little information regarding this issue exists in the literature. An overview of the problem has been given together with illustration of the effects on a compact single sided axial-flux PM machine. In particular the complexity of the problem has been outlined. It has also been shown that the bearing assembly requires a careful consideration, in particular if less common machine topology is considered.

A test procedure on a motor demonstrator has been described in detail. The approach utilises tests on the motor sub-assemblies to identify and quantity the mechanical loss components. These activities have been supplemented with CFD and equivalent circuit thermal modelling techniques to give more in depth insight into the mechanical and heat transfer effects related to the rotor sub-assembly. Limitations and uncertainties attributed with the methods used were illustrated and discussed.

IV.   REFERENCES

[1] F. Marignetti, V. Delli Colli, Y. Coia, "Design of Axial Flux PM Synchronous Machines Through 3-D Coupled Electromagnetic Thermal and Fluid-Dynamical Finite-Element Analysis," *IEEE Transactions on Industrial Electronics*, vol. 55, no. 10, pp. 3591–3601, October 2008.

[2] S. Scowby, R. Dobson, M. Kamper, "Thermal Modelling of an Axial Flux Permanent Magnet Machine," *Applied Thermal Engineering*, vol. 24, no. 2, pp. 193 – 207, February 2004.

[3] R. Wang, M. Kamper, R. Dobson, "Development of a Thermofluid Model for Axial Field Permanent-Magnet Machines," *Transactions on Energy Conversion, IEEE*, vol. 20, no. 1, pp. 80–87, March 2005.

[4] C. Lim, J. Bumby, R. Dominy, G. Ingram, K. Mahkamov, N. Brown, A. Mebarki, M. Shanel, "2-d Lumped-Parameter Thermal Modelling of Axial Flux Permanent Magnet Generator," *Proceedings of the 2008 International Conference on Electrical Machines (ICEM 2008)*, pp. 1 – 6, September 2008.

[5] G. Airoldi, G. Ingram, K. Mahkamov, J. Bumby, R. Dominy, N. Brown, A. Mebarki, and M. Shanel, "Computations on Heat Transfer in Axial Flux Permanent Magnet Machines," *Proceedings of the 2008 International Conference on Electrical Machines (ICEM 2008)*, pp. 1 – 6, September 2008.

[6] D. A. Howey, P. R. N. Childs, A. S. Holmes, "Air-Gap Convection in Rotating Machines," *IEEE Transactions on Industrial Electronics*, vol. 59, no. 3, pp. 1367 – 1375, March 2012.

[7] R. Camillieri, D. A. Howey, M. D. McCulloch, "Thermal Limitations in Air-Cooled Axial Flux In-Wheel Motors for Urban Mobility Vehicles: a Preliminary Analysis," *Conference on Electrical Systems for Aircraft, Railway and Ship Propulsion (ESARS 2012)*, pp. 1 – 8, October 2012.

[8] D. A. Howey, A. S. Holmes, K. R. Pullen, "Measurement and CFD Prediction of Heat Transfer in Air-Cooled Disc-Type Electrcal Machines," *IEEE Transactions on Industry Applications*, vol. 47, no. 4, pp. 1716 – 1723, August 2011.

[9] D. A. Howey, A. S. Holmes, K. R. Pullen, "Measurement of Stator Heat Transfer in Air-Cooled Axial Flux Permanent Magnet Machines," *35th IEEE Industrial Electronics Annual Conference (IECON 2009)*, pp. 1197 – 1202, November 2009.

[10] A. C. Malloy, R. F. Martinez-Botas, M. Jaensch, M. Lamperth "Measurement of Heat Generation Rate in Permanent Magnet Rotating Electrical Machines," *6th IET International Conference on Power Electronics, Machines and Drives (PEMD 2012)*, pp. 1 – 6, March 2012.

[11] D. Staton, A. Cavagnino, "Convection heat transfer and flow calculations suitable for electric machines thermal models," *IEEE Transactions on Industrial Electronics*, vol. 55, no. 10, pp. 3509 –3516, October 2008.

[12] R. Wrobel, P. H. Mellor, "A General Cuboidal Element for Three-Dimensional Thermal Modelling," *IEEE Transactions on Magnetics*, vol. 46, no. 8, pp. 3197 – 3200, August 2010.

[13] T. Synnot, "Mechanical Aspects of High Performance Electrical Machines – Hybrid Bearings for Integral Motors," *UK Magnetics Society One Day Seminar*, pp. 1-3, February 2013.

[14] T. A. Harris, M. N. Kotzalas, "Advanced Concepts of Bearing Technology – Rolling Bearing Analysis," *Taylor & Francis Group, CRC Press Book*, 2007.

[15] M. Calasan, M. Ostojic, D. Petrovic, "The retardation Method for Bearing Loss determination," *International Symposium on Power Electronics, Electrical Drives, Automation and Motion, (SPEEDAM 2012)*, pp. 25–29, June 2012.

[16] S. Marble, B. P. Morton, "Predicting the Remaining Life of Propulsion System Bearings," *IEEE Aerospace Conference*, pp. 1–8, March 2006.

[17] I. D. Ilina, "Experimental Determination of Moment of Inertia and Mechanical Loss vs. Speed, in Electrical Machines," *7th International Symposium on Advanced in Electrical Engineering, (ATEE 2011)*, pp. 1-4, May 2011.

[18] W. K. S. Khoo, K. Kalita, S. D. Garvey, "Practical Implementation of the Bridge Configured Winding for Producing Controllable Transverse Forces in Electrical Machines," *IEEE Transactions on Magnetics*, vol. 47, no. 6, pp. 1712-1718, June 2011.

[19] H-P. Liu, M. D. Werst, J. J. Hahne, D. Bogard, "Investigation of Windage Splits in an Enclosed Test Fixture Having a High-Speed Composite Rotor in Low Air Pressure Environments," *IEEE Transactions on Magnetics,* vol. 41, no. 1, pp. 316-321, January 2005.

[20] H-P. Liu, M. D. Werst, J. J. Hahne, D. Bogard, "Splits of Windage Losses in Integrated Transient Rotor and Stator Thermal Analysis of a High-Speed Alternator During Multiple Discharges," *IEEE Transactions on Magnetics*, vol. 41, no. 1, pp. 311-315, January 2005.

[21] P. H. Connor, S. J. Pickering, C. Gerada, C. N. Eastwick, C. Micallef, "CFD Modelling of an Entire Synchronous Generator for Improved Thermal Management," *6th IET International Conference Power Electronics, Machines and Drives, (PEMD 2012)*, pp. 1-6, March 2012.

[22] H. Hofmann, S. R. Sanders, "High-Speed Synchronous Reluctance Machine with Minimized Rotor Losses," *IEEE Transactions on Industry Applications*, vol. 36, no. 2, pp. 531–539, March/April 2000.

[23] G. J. Atkinson, B. C. Mecrow, A. G. Jack, D. J. Atkinson, P. Sangha, M. Benarous, "The Analysis of Loss in High-Power Fault-Tolerant Machines for Aerospace Applications," *IEEE Transactions on Industry Applications*, vol. 42, no. 5, pp. 1162–1170, September/October 2006.

[24] J. E. Vranick, "Prediction of Windage Power Loss in Alternators," *NASA Technical Note*, TN D-4849, pp. 1 – 18, October 1968.

[25] R. F. Handschuh, M. J. Hurrell, "Initial Experiments of High-Speed Drive System Windage Losses," *NASA Technical Note*, TM-2011-216925, pp. 1 – 17, November 2011.

[26] M. Saint Raymond, M. E. Kasarda, P. E. Allaire, "Windage Power Loss Modeling of a Smooth Rotor Supported by Homopolar Active Magnetic Bearings," *Journal of Tribology*, vol. 130, no. 2, pp. 1 – 8, September 2007.

[27] M. J. Hill, R. F. Kunz, R. B. Medvitz, R. F. Handschuh, L. N. Long, R. W. Noack, P. J. Morris, "CFD Analysis of Gear Windage Losses: Validation and Parametric Aerodynamic Studies," *Journal of Fluids Engineering*, vol. 133, no. 3, pp. 1 – 10, March 2011.

[28] R H. Jansen, T. P. Dever, "G2 Flywheel Module Design," NASA Technical Note, CR-2006-213862, pp. 1 – 20, August 2006.

[29] F. Chaari, M. Ben Romdhane, W. Baccar, T. Fakhfakh, M. Haddar, "Windage Power Loss in Spur Gear Sets," WSEAS Transactions on Applied and Theoretical Mechanics, vol. 7, no. 2, pp. 159 – 168, April 2012.

[30] G. K. Batchelor, "An Introduction to Fluid Dynamics," Cambridge University Press, 2005.

[31] L. Schouveiler, P. Le Gal, and MP Chauve. "Instabilities of the flow between a rotating and a stationary disk" *Journal of Fluid Mechanics*, vol. 443, pp. 329 – 350, 2001.

[32] J.W. Daily and R.E. Nece. "Chamber dimension effects on induced flow and frictional resistance of enclosed rotating disks" *ASME J. Basic Eng*, vol. 82, no. 1, pp. 217 – 232, 1960.

[33] D. Howey. "Thermal Design of Air Cooled Axial Flux Permanent Magnet Machines" Imperial College London PhD Thesis, March 2010.

[34] http://www.adapted-solutions.com